

V2X-Radar: A Multi-modal Dataset with 4D Radar for Cooperative Perception

Lei Yang¹, Xinyu Zhang^{1*}, Jun Li¹, Chen Wang², Zhiying Song¹, Tong Zhao¹, Ziying Song³
Li Wang¹, Mo Zhou¹, Yang Shen¹, Kai Wu⁴, Chen Lv⁵

¹ School of Vehicle and Mobility, Tsinghua University; ² China University of Mining and Technology

³ Beijing Jiaotong University; ⁴ ByteDance; ⁵ Nanyang Technological University

{yanglei20, song-zy24, zhaot20, wangli.thu, zhou-m21}@mails.tsinghua.edu.cn

{xyzhang, lijun1958}@tsinghua.edu.cn; songziying@bjtu.edu.cn; lyuchen@ntu.edu.sg



Figure 1. **A data frame sampled from V2X-Radar dataset.** Each sample consists of data from three distinct sensors: (1) Dense point clouds (gray points) from roadside and vehicle-side LiDAR. (2) Sparse point cloud (green / blue points) with doppler information from roadside and vehicle-side 4D Radar. (3) RGB images (top row) from vehicle’s camera and roadside multi-view cameras. All sensors have been synchronized in both time and spatial dimensions. The data frame is further annotated manually with 3D box across five categories, each category being represented by a unique color.

Abstract

Modern autonomous vehicle perception systems often struggle with occlusions and limited perception range. Previous studies have demonstrated the effectiveness of cooperative perception in extending the perception range and overcoming occlusions, thereby improving the safety of autonomous driving. In recent years, a series of cooperative perception datasets have emerged. However, these datasets only fo-

cus on camera and LiDAR, overlooking 4D Radar, a sensor employed in single-vehicle autonomous driving for robust perception in adverse weather conditions. In this paper, to bridge the gap of missing 4D Radar datasets in cooperative perception, we present V2X-Radar, the first large real-world multi-modal dataset featuring 4D Radar. Our V2X-Radar dataset is collected using a connected vehicle Radar, LiDAR, and multi-view cameras. The collected data includes sunny and rainy weather conditions, spanning daytime, dusk, and nighttime, as well as typical challenging

*Corresponding Author.

scenarios. The dataset comprises 20K LiDAR frames, 40K camera images, and 20K 4D Radar data, with 350K annotated bounding boxes across five categories. To facilitate diverse research domains, we establish V2X-Radar-C for cooperative perception, V2X-Radar-I for roadside perception, and V2X-Radar-V for single-vehicle perception. We further provide comprehensive benchmarks of recent perception algorithms on the above three sub-datasets. The dataset and benchmark codebase will be available at: <http://openmpd.com/column/V2X-Radar>.

1. Introduction

Perception is critical in autonomous driving, and while a lot of single-vehicle perception methods [12, 14, 20, 22, 24–26, 39, 48] have emerged, it still faces substantial safety challenges arising from occlusions and limited perception ranges. These issues arise because vehicles can only see their surroundings from a single view, leading to an incomplete scenario perception. This limitation hinders autonomous vehicles from achieving safe navigation and making optimal decisions. To address this limitation, recent works have delved into the vehicle-to-everything (V2X) cooperative perception, where the ego vehicle utilizes the information from other agents through wireless communication to extend perception range and overcome occlusions.

Recently, cooperative perception has gained increasing attention, and several pioneering datasets have been released to support this research. For instance, datasets like OpenV2V [33], V2X-Sim [10], and V2XSet [32] are generated through simulations using CARLA [3] and SUMO [8]. Conversely, datasets such as DAIR-V2X [42], V2X-Seq [43], V2V4Real [35], and V2X-Real [28] are derived from real-world scenarios. However, a shared limitation of these datasets is their exclusive focus on camera and LiDAR sensors, overlooking the potential of 4D Radar. This sensor is considered helpful to robust perception for its exceptional adaptability to adverse weathers, which has been validated in the single-vehicle autonomous driving datasets such as K-Radar [17] and Dual-Radar [46].

In order to fill the gap of missing 4D Radar dataset in the field of cooperative perception and thus facilitate related studies, we present V2X-Radar, the first large real-world multi-modal dataset with 4D Radar. This dataset comprises a wide variety of scenarios, encompassing various weather conditions such as sunshine, rain and snow, spanning different times of the day including daytime, dusk, and nighttime. The data is collected using a connected vehicle platform and an intelligent roadside unit, both equipped with 4D Radar, LiDAR, and multi-view cameras (Fig. 1). From over 15 hours of collected driving logs, we carefully selected 50 representative scenarios for the final dataset. It comprises 20K LiDAR frames, 40K camera images, and

20K 4D Radar data, featuring 350K annotated bounding boxes across 5 object categories. To support a variety of research areas, the V2X-Radar is further divided into three specialized sub-datasets: V2X-Radar-C for cooperative perception, V2X-Radar-I for roadside perception, and V2X-Radar-V for single-vehicle perception. Additionally, we provide comprehensive benchmarks of recent perception algorithms across these three sub-datasets. Compared to the existing real-world cooperative datasets, our V2X-Radar shows two strengths: (1) **More modalities**: The proposed V2X-Radar dataset includes three types of sensors: LiDAR, Camera, and 4D Radar, enabling further exploration into 4D Radar-related cooperative perception research. (2) **Diverse scenarios**: Our data collection encompasses various weather conditions and times of day, while also focuses on challenging intersections for single-vehicle autonomous driving. These intersections have obstructed blind spots that significantly impact vehicle safety, providing diverse corner cases for cooperative perception research.

Our contributions can be summarized as follows:

- We build V2X-Radar, the first large real-world multi-modal dataset featuring 4D Radar tailored for cooperative perception. All the frames are captured through diverse real-world scenarios using multi-modal sensors.
- We provide 20K LiDAR frames, 40K multi-view camera images, and 20K 4D Radar data, alongside 350K annotated bounding boxes spanning five object categories.
- Comprehensive benchmarks of recent perception algorithms are conducted across cooperative perception on V2X-Radar-C, roadside perception on V2X-Radar-I, and vehicle-side perception on V2X-Radar-V. We will release all the V2X-Radar dataset and benchmark codebase.

2. Related Works

2.1. Autonomous Driving Datasets

Public datasets [1, 10, 17, 23, 28, 32, 33, 35, 42, 43, 46, 47] have greatly accelerated the progress of autonomous driving in recent years. See Tab. 1 for a summary of autonomous driving datasets. Single-vehicle datasets, such as KITTI [5], NuScenes [1], and Waymo [23], have significantly promoted the development of single-vehicle perception. For the sake of cooperative perception datasets, OPV2V [33] is the first dataset in this field. It collects data through CARLA [3] and OpenCDA [30, 34] co-simulation. V2XSet [32] and V2X-Sim [10] explore V2X perception using synthesized data from the CARLA simulator [3]. In contrast to simulated datasets, DAIR-V2X introduces the first real-world dataset for cooperative detection. V2X-Seq [43] extends sequences from DAIR-V2X [42] with track IDs, creating a sequential perception and trajectory forecasting dataset. V2V4Real [35] presents the initial real-world V2V dataset collected by two connected

Table 1. Comparisons of our proposed V2X-Radar with existing autonomous driving and V2X datasets. C: Camera, L: Lidar, R: Radar, V2V: vehicle-to-vehicle, V2I: Vehicle-to-infrastructure.

Dataset	Year	Location	Sensor	V2X	Multi-view Cameras	Real Data	4D Radar
KITTI [5]	2012	Germany	L&C	✗	✗	✓	✗
Waymo [23]	2019	USA	L&C	✗	✓	✓	✗
nuScenes [1]	2019	USA	L&C&R	✗	✓	✓	✗
OpenV2V [33]	2022	Carla	L&C	V2V	✓	✗	✗
V2X-Sim [10]	2022	Carla	L&C	V2V&I	✓	✗	✗
V2X-Set [32]	2022	Carla	L&C	V2V&I	✓	✗	✗
DAIR-V2X [42]	2022	China	L&C	V2I	✗	✓	✗
V2X-Seq [43]	2023	China	L&C	V2I	✗	✓	✗
V2V4Real [35]	2023	USA	L&C	V2V	✓	✓	✗
V2X-Real [28]	2024	USA	L&C	V2V&I	✓	✓	✗
TUMTraf-V2X [50]	2024	Germany	L&C	V2I	✓	✓	✗
V2X-Radar (Ours)	2024	China	L&C&R	V2I	✓	✓	✓

vehicles. V2X-Real [28] is a large-scale multi-modal multi-view dataset designed for V2X research, gathered using two connected automated vehicles and two intelligent roadside units. A common limitation among the above cooperative perception datasets is their emphasis solely on camera and LiDAR sensors, overlooking the capabilities of 4D Radar. 4D Radar is known for its superior adaptability to adverse weather conditions, which has been proven by single-vehicle autonomous driving datasets like K-Radar [17] and Dual-Radar [46]. Therefore, it is crucial to introduce a real-world cooperative dataset incorporating 4D Radar to fill this gap and further facilitate 4D Radar-related cooperative perception research.

2.2. Cooperative Perception

Cooperative perception aims to extend the perception range and overcome occlusions in single-vehicle perception by leveraging the shared information among connected agents. It can be classified into three main types based on fusion strategies.: (1) Early Fusion, which involves transmitting raw sensor data for the ego-vehicle to aggregate and predict objects. (2) Late Fusion that integrates detection results for a consistent prediction. (3) Intermediate Fusion that shares and fuses intermediate high-level features.

Recent state-of-the-art methods [2, 4, 6, 16, 27, 27, 31, 32, 44, 45, 49] typically follow the intermediate fusion, which achieves the best trade-off between accuracy and bandwidth requirements. For instance, V2VNet [27] utilized graph neural networks for integrating intermediate features. F-Cooper [2] applied max-pooling fusion to merge shared voxel features. CoBEVT [31] introduced local-global sparse attention for improved cooperative BEV map segmentation. V2X-ViT [32] presented a unified vision transformer for multi-agent and multi-scale perception. HM-ViT [6] introduced a 3D heterogeneous graph transformer for camera and LiDAR fusion. HEAL [16] proposed

an extensible collaborative perception framework to integrate new heterogeneous agents with minimal integration cost and performance decline.

3. V2X-Radar Dataset

To facilitate the cooperative perception research with 4D Radar, we present V2X-Radar, the first large real-world multi-modal dataset featuring 4D Radar. In this section, we first detail the data acquisition in Sec. 3.1, then present the data annotation in Sec. 3.2, and finally delve into the diverse data distribution and dataset analysis in Sec. 3.3.

3.1. Data Acquisition

Sensor Setup. The dataset was collected using a connected vehicle-side platform (Fig. 2(a)) and an intelligent roadside unit (Fig. 2(b)). Both are equipped with sensors such as 4D Radar, LiDAR, and multi-view cameras. Additionally, the GPS/IMU system is employed to achieve high-precision localization, which serves for the initial point cloud registration between vehicle-side and roadside platforms. C-V2X unit is also integrated for wireless data transmission. The sensor layout configuration can be found in Fig. 2, and detailed specifications are listed in Tab. 2.

Synchronization. For cooperative perception datasets, it is crucial to synchronize sensors on both vehicle-side and roadside platforms using a uniform timestamp standard. To ensure consistency, all computer clocks are first aligned with GPS time. Hardware-triggered synchronization of LiDAR, cameras, and 4D Radar is then implemented using the Precision Time Protocol (PTP) and Pulse Per Second (PPS) signals. Subsequently, the closest LiDAR frames from the vehicle-side and roadside platforms are matched, and camera and 4D Radar data are aligned with each corresponding LiDAR frame to create unified multi-modal data frames. Finally, the time difference between sensors across

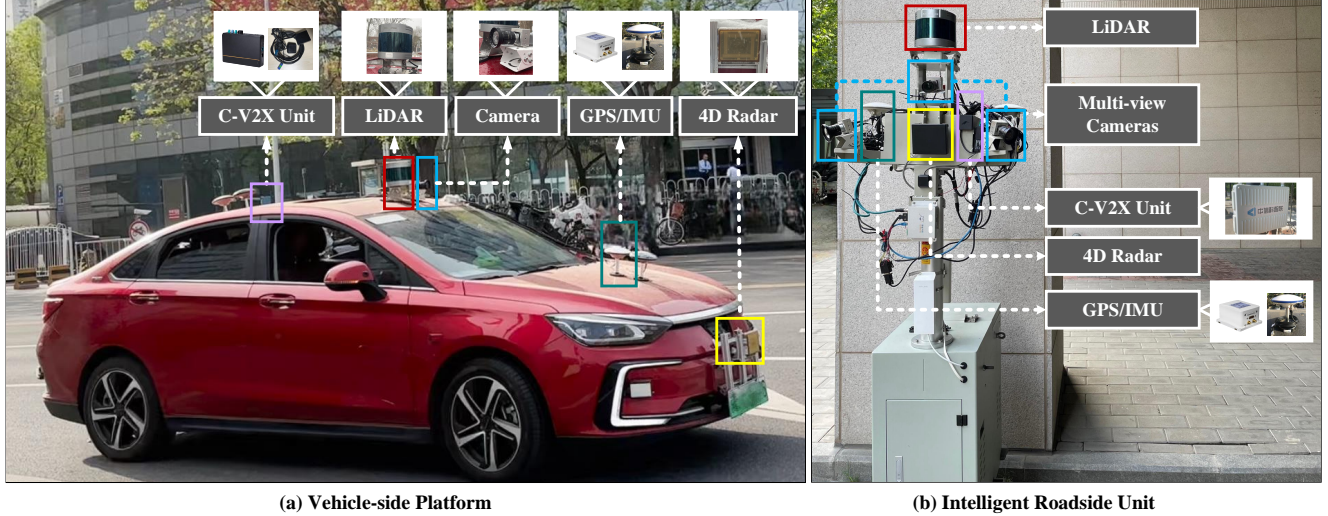


Figure 2. **The sensor configuration on the connected vehicle-side platform and the intelligent roadside unit.** a) The vehicle-side platform. b) The intelligent roadside unit or infrastructure unit. Both of them are equipped with multi-modal sensors including camera, LiDAR and 4D Radar, along with a C-V2X unit and a GPS/IMU system.

Table 2. **Sensor specifications in V2X-Radar dataset.** ‘Infra.’ means infrastructure or intelligent roadside unit.

Agent	Sensor	Sensor Model	Details
Infra.	LiDAR	RoboSense RS-Ruby-80 ($\times 1$)	80 beams, 360° horizontal FOV, -25° to $+25^\circ$ vertical FOV
	Camera	Basler acA1920-40gc ($\times 3$)	RGB, 1536 \times 864 resolution
	4D Radar	OCULI EAGLE ($\times 1$)	79.0GHz, -56° to $+56^\circ$ horizontal FOV, -22° to $+22^\circ$ vertical FOV
	C-V2X Unit	VU4004 ($\times 1$)	PC5/4G LTE/V2X Protocol
	GPS/IMU	XW-GI5651 ($\times 1$)	1000Hz update rate, Double-Precision
Vehicle	LiDAR	RoboSense RS-Ruby-80 ($\times 1$)	80 beams, 360° horizontal FOV, -25° to $+25^\circ$ vertical FOV
	Camera	Basler acA1920-40gc ($\times 1$)	RGB, 1920 \times 1080 resolution
	4D Radar	Arbe Phoenix ($\times 1$)	77GHz, -50° to $+50^\circ$ horizontal FOV, -15° to $+15^\circ$ vertical FOV
	C-V2X Unit	VU4004 ($\times 1$)	PC5/4G LTE/V2X Protocol
	GPS/IMU	XW-GI5651 ($\times 1$)	1000Hz update rate, Double-Precision

the two platforms is maintained below 50 milliseconds for each sample.

Sensor Calibration and Registration. Through the sensor calibration process, we achieve spatial synchronization of the camera, LiDAR, and 4D Radar. The intrinsic parameters of the camera are calibrated using a checkerboard pattern. In contrast, the LiDAR is calibrated relative to the camera by utilizing 100 point pairs extracted from the point cloud and the corresponding camera image. The extrinsic parameters are derived by minimizing the reprojection errors between the 2D-3D point correspondences. The calibration of the LiDAR with the 4D Radar is performed by selecting 100 high-intensity point pairs located on corner reflectors. The results of this calibration are visually represented in Fig. 3. Vehicle-side LiDAR alignment with roadside LiDAR is achieved through point cloud registration, initially computed using RTK localization and subsequently refined via CBM [21] and manual adjustments. The visualization

of the point cloud registration is shown in Fig. 4.

Data Collection. We collected 15 hours of driving data with 540K frames, capturing various weather conditions such as sunny and rainy, spanning daytime, dusk, and nighttime, as well as typical challenging intersection scenarios. Further details can be found in the supplementary materials. From this, we manually select the most representative 40 sequences to form V2X-Radar-C; each sequence is 10-25 seconds long with a 10Hz capturing frequency. On this basis, we additionally sample 10 vehicle-only sequences to create V2X-Radar-V and sample an additional 10 infrastructure-only sequences to form V2X-Radar-I. In comparison to the single-view data in V2X-Radar-C, both V2X-Radar-V and V2X-Radar-I encompass more diverse scenes. Consequently, the above three sub-datasets collectively encompassed 20K LiDAR frames, 40K camera images, and 20K 4D Radar data.

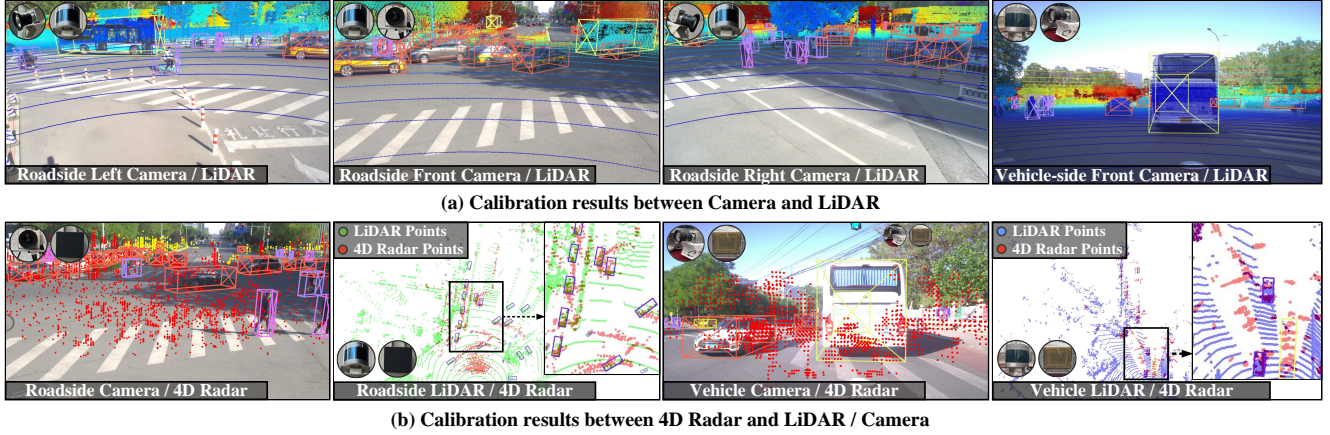


Figure 3. **Visualization of calibration results.** a) The calibration results between the camera and LiDAR. b) The calibration results between 4D Radar and LiDAR / Camera. The LiDAR points are projected onto the camera plane using camera intrinsics and camera-LiDAR extrinsic. Similarly, the 4D Radar points are transferred onto the LiDAR coordinate system using the 4D Radar-LiDAR extrinsic. Additionally, these 4D Radar points are also mapped onto the camera plane by leveraging the camera’s intrinsic parameters, along with the extrinsic parameters of camera-LiDAR and 4D Radar-LiDAR.

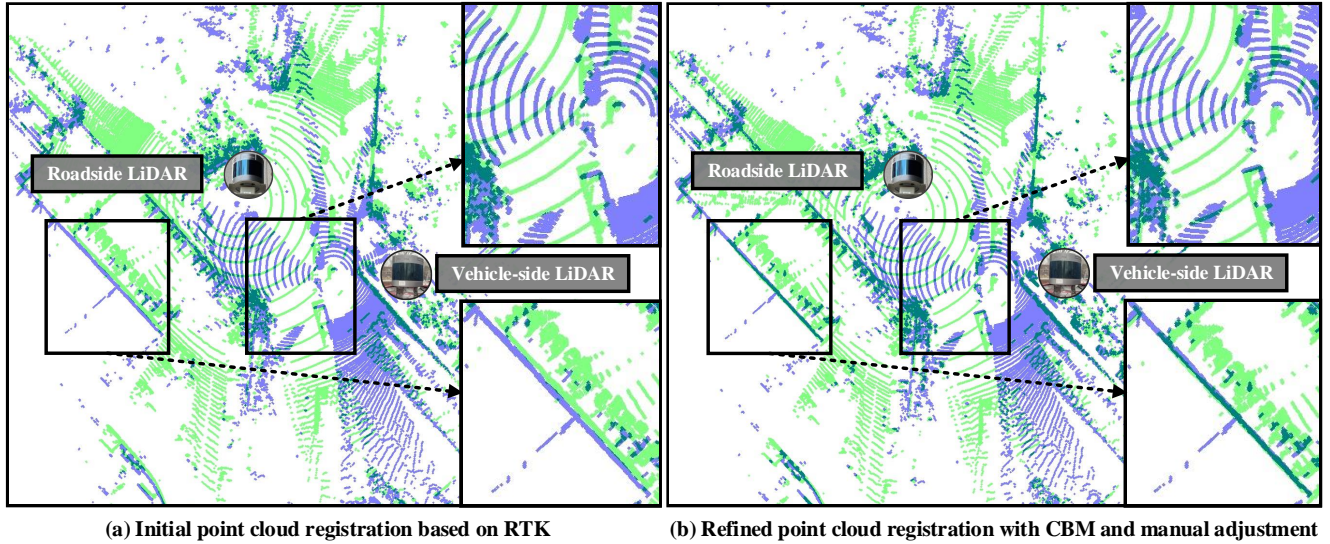


Figure 4. **Visualization of point cloud registration results.** a) Initial point cloud registration based on RTK localization. b) Refined point cloud registration with CBM [21] and manual adjustment. The blue points represent the point cloud from the vehicle-side LiDAR, while the green points indicate the point cloud from the roadside LiDAR.

3.2. Data Annotation.

Coordinate System. Our dataset comprises four types of coordinate systems: (1) LiDAR coordinate system, where the X, Y, and Z axes align with the front, left, and upward directions of the LiDAR. (2) Camera coordinate systems, where the z-axis denotes depth. (3) 4D Radar coordinate system, where the X, Y, and Z axes are oriented towards the right, front, and upward directions. (4) Global coordinate system, which maintains consistency with the LiDAR frame on the roadside platform.

3D Bounding Boxes Annotation.

Data annotation includes annotations for vehicles, road-sides, and collaborative efforts. Vehicle and roadside annotations are manually created within their specific LiDAR coordinate systems. For the collaborative annotation, we first align the vehicle-side and roadside annotations within a unified roadside LiDAR coordinate system, then match them using the Intersection over Union (IoU) metric to eliminate duplicates. The annotation process involves five object categories: pedestrian, cyclist, car, bus, and truck. Each object annotation includes attributes such as occlusion and truncation, as well as the geometric properties of 3D bounding boxes, denoted as $(x, y, z, w, h, l, \theta)$, where (l, w, h) repre-

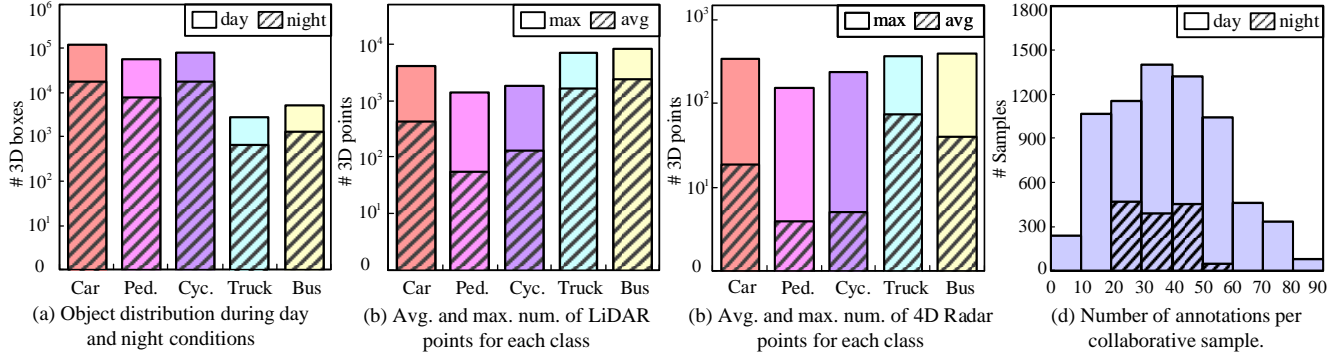


Figure 5. **Data analysis of our V2X-Radar dataset.** a) Objects distribution during day and night conditions. b) Average and maximum number of LiDAR points within the 3D bounding box for each category. c) Average and maximum number of 4D Radar points within the 3D bounding box for each category. d) Number of annotations per collaborative sample. The vertical axes of sub-plots (a)-(c) employ a log scale, while the vertical axis of sub-plot (d) utilizes a standard scale.

sent the object’s dimensions, (x, y, z) indicate its location, and θ denotes its orientation.

3.3. Data Analysis

Fig. 5(a) shows the distribution of objects across five categories in day and night conditions, with cars being the most common in V2X-Radar, followed by cyclists and pedestrians, while trucks and buses are the least frequent. Fig. 5(b) presents the maximum and average number of LiDAR points within 3D bounding boxes for each category, indicating that larger vehicles have more 3D points than smaller pedestrians or cyclists. Fig. 5(c) reveals the density distribution of 4D Radar points within different object’s bounding boxes, mirroring a similar trend to Fig. 5(b). Lastly, Fig. 5(d) demonstrates that annotations per collaborative sample can reach up to 90 - significantly higher than single-vehicle datasets like KITTI [5] or nuScenes [1], highlighting how combining vehicle-side and roadside data enhances environmental perception comprehensiveness.

4. Tasks

Our V2X-Radar dataset, comprising of three subsets: V2X-Radar-I, V2X-Radar-V, and V2X-Radar-C, is designed to facilitate roadside 3D object detection, single-vehicle 3D object detection, and cooperative 3D object detection.

4.1. Single-agent 3D Object Detection

Task Definition. Single-agent 3D object detection involves two tasks: roadside 3D object detection using the V2X-Radar-I sub-dataset and vehicle-side 3D object detection using the V2X-Radar-V sub-dataset. These tasks rely on sensors from either the intelligent roadside unit or the vehicle-side platform for detecting 3D objects, leading to the following challenges:

- **Single-modal Encoding:** The process of encoding 2D image from the camera, dense 3D point cloud from Li-

DAR, sparse point cloud with Doppler information from 4D Radar into 3D spatial representation is necessary for precise single-modal 3D object detection.

- **Multi-modal Fusion:** When fusing multi-modal information from different sensors, it is necessary to consider (1) spatial misalignment, (2) temporal misalignment, and (3) sensor failure. These issues are necessary to achieve robust multi-modal 3D object detection.

Evaluation Metrics. The evaluation area covers $[-100, 100]$ in the x direction and $[0, 100]$ in the y direction from the ego-vehicle or roadside unit. Following the metrics in Rope3D [40], KITTI [5] datasets, we utilize the Average Precision (AP) at IoU thresholds of 0.5 and 0.7 to evaluate the performance of object detection.

Benchmark Methods. We extensively evaluate various leading single-agent 3D object detectors based on different sensor inputs. In particular, our evaluation encompasses LiDAR-centric techniques such as PointPillars [9], SECOND [36], CenterPoint [41], and PV-RCNN [19]; camera-dependent methods including SMOKE [13], BVDepth [11], BEVHeight [38], and BEVHeight++ [37]; and 4D Radar-based approaches like RPFA-Net [29] and RDIoU [18].

4.2. Cooperative 3D Object Detection

Task Definition. The goal of the cooperative 3D object detection task using the V2X-Radar-C sub-dataset is to utilize sensors from both the vehicle and intelligent roadside unit for ego-vehicle’s 3D object detection. Unlike previous single-agent perception, cooperative perception presents unique domain-specific challenges:

- **Spatial Asynchrony:** Localization errors can create discrepancies in the relative position between the single-vehicle platform and the intelligent roadside unit, potentially leading to global misalignment when translating data from the roadside unit to the ego-vehicle coordinate system.

Table 3. **Roadside 3D object detection benchmarks on V2X-Radar-I under homogeneous split.** The vehicle category includes car, bus and truck. ‘M’ means modality, and L, C, R denotes LiDAR, Camera and 4D Radar respectively.

Method	M	Vehicle (IoU = 0.7 / 0.5)			Pedestrian (IoU = 0.5 / 0.25)			Cyclist (IoU = 0.5 / 0.25)		
		Easy	Moderate	Hard	Easy	Moderate	Hard	Easy	Moderate	Hard
Pointpillars [9]	L	78.00 / 88.69	71.24 / 81.16	71.24 / 81.16	53.87 / 69.61	52.94 / 67.09	52.94 / 67.09	80.01 / 87.48	72.67 / 78.60	72.67 / 78.60
SECOND [36]	L	81.61 / 91.06	74.34 / 83.47	74.34 / 83.47	57.56 / 74.64	55.39 / 72.27	55.39 / 72.27	80.53 / 87.68	74.06 / 80.62	74.06 / 80.62
CenterPoint [41]	L	86.44 / 94.04	78.98 / 84.26	78.98 / 84.26	67.90 / 84.74	65.39 / 81.35	65.39 / 81.35	90.26 / 92.91	82.87 / 85.51	82.87 / 85.51
PV-RCNN [19]	L	88.83 / 94.11	81.39 / 86.61	81.39 / 86.61	77.13 / 86.39	74.66 / 83.87	74.66 / 83.87	91.82 / 94.44	84.47 / 87.08	84.46 / 87.08
SMOKE [13]	C	22.05 / 58.43	20.72 / 56.36	20.69 / 56.31	8.26 / 25.64	7.68 / 24.36	7.63 / 24.30	12.50 / 38.29	11.28 / 36.40	11.24 / 36.36
BEVDepth [11]	C	45.01 / 69.25	42.23 / 66.81	42.21 / 66.75	30.64 / 61.46	29.13 / 59.11	29.10 / 59.05	39.85 / 68.71	38.52 / 67.05	38.43 / 67.02
BEVHeight [38]	C	47.91 / 72.45	45.53 / 69.48	45.49 / 67.44	32.08 / 64.06	29.78 / 59.79	29.68 / 59.74	42.97 / 71.63	41.34 / 69.11	41.30 / 69.07
BEVHeight++ [37]	C	48.48 / 73.81	47.92 / 70.36	47.88 / 70.32	33.05 / 66.12	32.30 / 64.67	32.32 / 64.66	45.19 / 74.52	44.20 / 72.04	44.14 / 72.01
RDIoU [18]	R	61.38 / 80.03	54.89 / 72.72	54.89 / 72.72	43.82 / 72.03	42.11 / 69.65	42.11 / 69.65	40.74 / 67.31	36.68 / 60.83	36.68 / 60.83
RPFA-Net [29]	R	64.79 / 82.58	58.01 / 75.36	58.01 / 75.36	51.64 / 78.05	49.51 / 73.91	49.51 / 73.91	45.86 / 71.81	41.66 / 64.95	41.66 / 64.95

Table 4. **Single-vehicle 3D object detection benchmarks on V2X-Radar-V under homogeneous split.** The vehicle category includes car, bus and truck. ‘M’ means modality, and L, C, R denotes LiDAR, Camera and 4D Radar respectively.

Method	M	Vehicle (IoU = 0.7 / 0.5)			Pedestrian (IoU = 0.5 / 0.25)			Cyclist (IoU = 0.5 / 0.25)		
		Easy	Moderate	Hard	Easy	Moderate	Hard	Easy	Moderate	Hard
Pointpillars [9]	L	75.66 / 83.52	68.80 / 77.07	68.80 / 77.07	41.89 / 46.34	38.16 / 43.18	38.16 / 43.18	78.63 / 83.14	65.24 / 69.77	65.24 / 69.77
SECOND [36]	L	78.35 / 84.34	71.31 / 79.75	71.31 / 79.75	43.74 / 49.75	39.07 / 45.91	39.07 / 45.91	82.88 / 85.12	68.27 / 73.22	68.27 / 73.22
CenterPoint [41]	L	80.87 / 87.74	72.19 / 81.42	72.19 / 81.42	55.27 / 62.63	50.59 / 58.81	50.59 / 58.81	88.21 / 92.48	75.26 / 79.44	75.26 / 79.44
PV-RCNN [19]	L	88.27 / 89.12	79.38 / 84.31	79.38 / 84.31	67.04 / 69.81	58.83 / 65.78	58.83 / 65.78	89.48 / 93.49	78.01 / 81.07	78.01 / 81.07
SMOKE [13]	C	9.86 / 31.92	8.61 / 26.41	8.28 / 24.36	0.23 / 2.02	0.29 / 1.89	0.29 / 1.89	0.39 / 7.23	0.37 / 4.96	0.37 / 4.13
BEVDepth [11]	C	16.91 / 41.63	15.47 / 39.68	15.02 / 37.83	9.92 / 29.98	8.51 / 27.76	8.49 / 27.72	12.18 / 47.20	9.46 / 39.34	9.30 / 39.15
BEVHeight [38]	C	16.58 / 40.32	15.32 / 39.15	14.08 / 37.30	9.49 / 28.50	8.48 / 26.46	8.39 / 26.57	9.58 / 44.56	7.35 / 35.04	7.26 / 34.91
BEVHeight++ [37]	C	17.47 / 43.68	15.53 / 42.24	14.77 / 41.58	10.43 / 31.15	9.36 / 28.85	9.32 / 28.73	12.99 / 49.08	9.91 / 41.10	9.83 / 40.94
RDIoU [18]	R	41.11 / 72.67	29.03 / 54.27	28.37 / 52.02	10.72 / 28.59	9.97 / 26.88	9.84 / 26.78	14.74 / 44.57	10.81 / 31.15	10.67 / 30.91
RPFA-Net [29]	R	42.77 / 75.79	30.44 / 57.27	29.34 / 55.06	11.51 / 30.54	10.37 / 28.15	10.29 / 27.43	17.03 / 46.31	11.98 / 33.96	11.91 / 33.77

- **Temporal Asynchrony:** Communication delays in data transmission can result in timestamp discrepancies between sensor data from the single-vehicle platform and the intelligent roadside unit. This may cause local misalignment of dynamic objects when translating data within the same coordinate system.

Evaluation Metrics. The evaluation area covers [-100, 100] meters in both the x and y directions with respect to the ego vehicle. Similar to DAIR-V2X [42] and V2V4Real [35], We group various vehicle types into the same class and focus solely on vehicle detection. The object detection performance is evaluated by Average Precision (AP) at IoU thresholds of 0.5 and 0.7. Transmission costs are measured through Average MegaBytes (AM). Following prior studies [35, 42], we compare methods in two setups: (1) Synchronous, ignoring communication delays. (2) Asynchronous, with a 100 ms delay simulated by fetching the roadside sensor data with the previous timestamp.

Benchmark Methods. We present comprehensive benchmarks for the following three fusion strategies in cooperative 3D object detection:

- **Late Fusion:** Each agent utilizes its sensors to detect 3D

objects and shares the predictions. The receiving agent then applies NMS to produce the final outputs.

- **Early Fusion:** The ego-vehicle gathers all the point clouds both from itself and other agents to its own coordinate system, then proceeds with detection procedures.
- **Intermediate Fusion:** Each agent uses a neural feature extractor to obtain intermediate features, which are then compressed and sent to the ego vehicle for cooperative feature fusion. We evaluate several leading methods, including F-Cooper [2], V2XVIT [32], CoAlign [31], and HEAL [16], to establish a benchmark in this field.

5. Experiments

5.1. Implementation details

For the dataset split, single-agent 3D object detection, including roadside and vehicle-side scenarios, adheres to two distinct setups: (1) homogeneous split, the dataset is divided into train/val/test with 7000, 1500, and 1500 frames, respectively. It is crucial to highlight that the selection of samples in this setup is completely random. (2) heterogeneous split, the dataset is divided into train/val/test with 34, 8, and 8

Table 5. **Cooperative 3D object detection benchmarks for vehicle category on V2X-Radar-C.** The vehicle category includes car, bus and truck. Sync. means synchronous setup ignoring communication delays. Async. implies asynchronous setup with a 100 ms delay.

Method	M	Sync. (AP@IoU = 0.5 / 0.7)				Async. (AP@IoU = 0.5 / 0.7)				AM (MB)
		Overall	0-30m	30-50m	50-100m	Overall	0-30m	30-50m	50-100m	
No Fusion	L	21.44 / 17.40	22.73 / 18.54	22.22 / 18.60	18.15 / 13.64	21.44 / 17.40	22.73 / 18.54	22.22 / 18.60	18.15 / 13.64	0
Late Fusion	L	54.38 / 35.03	67.09 / 52.93	49.56 / 35.46	32.58 / 20.51	47.84 / 22.11	59.97 / 33.13	42.05 / 20.84	28.27 / 14.78	0.003
Early Fusion	L	58.89 / 49.04	74.13 / 63.74	52.73 / 43.64	34.38 / 28.71	51.09 / 27.22	64.38 / 35.67	43.26 / 22.05	29.93 / 19.08	1.25
F-Cooper [2]	L	60.27 / 45.33	74.91 / 61.87	56.64 / 38.95	35.85 / 21.32	55.56 / 32.03	70.11 / 44.81	50.01 / 23.64	32.48 / 17.31	0.25
CoAlign [15]	L	66.42 / 55.56	70.81 / 63.27	66.75 / 54.15	58.36 / 43.01	58.43 / 35.07	63.32 / 39.61	56.64 / 31.83	50.65 / 31.00	0.25
HEAL [16]	L	67.75 / 57.78	72.78 / 65.59	69.24 / 56.23	57.79 / 45.32	60.75 / 39.27	65.72 / 43.95	59.99 / 36.04	51.41 / 34.52	0.25
No Fusion	C	3.45 / 2.61	5.08 / 1.56	0.69 / 0.29	0.22 / 0.10	3.45 / 2.61	5.08 / 1.56	0.69 / 0.29	0.22 / 0.10	0
Late Fusion	C	12.82 / 7.56	27.33 / 16.53	2.38 / 1.93	1.87 / 0.92	11.08 / 4.68	23.88 / 10.19	1.94 / 1.14	1.59 / 0.58	0.003
V2X-ViT [32]	C	17.51 / 10.54	32.28 / 19.93	3.42 / 2.64	2.34 / 1.39	15.61 / 7.24	29.19 / 13.58	2.95 / 1.71	2.05 / 0.92	0.25
CoAlign [15]	C	19.33 / 12.67	37.01 / 21.05	3.89 / 2.73	2.45 / 1.41	17.33 / 8.61	33.41 / 14.11	3.27 / 1.74	2.17 / 0.97	0.25
HEAL [16]	C	19.58 / 13.56	34.74 / 24.84	4.02 / 2.88	2.80 / 1.53	17.42 / 9.53	31.23 / 17.43	3.43 / 1.96	2.47 / 0.98	0.25
No Fusion	R	6.98 / 3.06	11.63 / 6.62	1.08 / 0.52	0.87 / 0.26	6.98 / 3.06	11.63 / 6.62	1.08 / 0.52	0.87 / 0.26	0
Late Fusion	R	10.95 / 6.87	20.59 / 11.69	1.93 / 1.15	1.21 / 0.54	9.76 / 4.67	18.39 / 7.83	1.44 / 0.74	1.06 / 0.41	0.003
Early Fusion	R	13.65 / 7.37	24.07 / 13.89	2.19 / 1.49	1.25 / 0.71	12.09 / 5.24	21.51 / 9.76	1.67 / 1.01	1.09 / 0.46	0.32
V2X-ViT [32]	R	14.23 / 8.74	25.23 / 14.92	2.84 / 1.77	1.66 / 0.93	12.68 / 6.01	22.82 / 10.17	2.25 / 1.15	1.46 / 0.61	0.25
CoAlign [15]	R	15.59 / 9.76	26.76 / 17.32	3.08 / 1.86	2.05 / 1.23	13.71 / 6.52	23.63 / 11.49	2.41 / 1.16	1.77 / 0.82	0.25
HEAL [16]	R	15.82 / 10.08	27.02 / 18.24	3.56 / 1.91	1.83 / 1.12	13.97 / 7.56	24.11 / 12.97	2.85 / 1.23	1.62 / 0.75	0.25

sequences, respectively. The dataset for cooperative 3D object detection is divided into train/val/test with 30, 5, and 5 sequences, respectively. In particular, all experimental results are evaluated using the validation set. For the detection areas, the single-agent detection techniques span a range of [0, 100]m in the x-direction and [-100, 100]m in the y-direction relative to the ego vehicle or roadside unit. On the other hand, cooperative 3D object detection encompasses a broader area, covering [-100, 100]m in both the x and y directions. For the ground truth, LiDAR or camera methods use all the annotations. Considering the limited coverage area of 4D Radar, 4D Radar-based methods only use labels located within its field of view. For the feature extractor, all the cooperative detection methods rely on PointPillar [9] to extract BEV features from LiDAR or 4D Radar point clouds and utilize BEVDet [7] to extract BEV features from camera images.

5.2. Benchmark results

Single-agent 3D Object Detection. The benchmark results for the V2X-Radar-I and V2X-Radar-V sub-datasets under a homogeneous split are presented in Tab. 3 and Tab. 4. Additional results under the heterogeneous split can be found in the supplementary materials. The experimental results in these tables clearly illustrate that LiDAR-based methods achieve the most superior performance. 4D radar-based methods, although they deal with a relatively sparse point cloud, still perform better than camera-based methods. Camera-based methods, hindered by their inability to utilize depth information, are less effective than LiDAR and 4D Radar-based methods.

Cooperative 3D Object Detection. Tab. 5 demonstrates a

quantitative comparison among several methods on V2X-Radar-C. We can observe that:

- Compared to the baseline of single-vehicle perception, all methods involving cooperative perception exhibit a significant performance improvement, highlighting its key role in boosting single-vehicle perception.
- Compared to the synchronous setting results, introducing communication delay in asynchronous settings caused a significant drop in Average Precision (AP) across all methods. For example, with a strict IoU of 0.7, F-Cooper [2], CoAlign [15], and HEAL [16] using LiDAR point clouds experienced substantial decreases of 13.30%, 20.49%, and 18.51%, respectively. These findings underscore the necessity of mitigating the impact of communication delay in robust cooperative perception.

6. Conclusion

In this paper, we introduce V2X-Radar, the first large real-world multi-modal dataset featuring 4D Radar for cooperative perception, aiming to prompt cooperative perception research with 4D Radar for a broader operational design domain (ODD). Our dataset focuses on challenging intersection scenarios and provides data collected from diverse times and weather conditions. It comprises 20K LiDAR frames, 40K camera images, and 20K 4D Radar data points, with 350K annotated bounding boxes spanning 5 categories. To facilitate a wide range of perception research, we structure the dataset into three sub-datasets: V2X-Radar-C for cooperative perception, V2X-Radar-I for roadside perception, and V2X-Radar-V for single-vehicle perception. Furthermore, we have conducted extensive benchmarks of recent perception algorithms on these three sub-datasets.

Limitation and Future Work. Our dataset primarily focuses on 3D object detection, while the asynchronous setting in cooperative perception evaluation is simulated with a fixed time delay. In the future, we plan to expand our tasks based on V2X-Radar to include tracking and trajectory prediction, and we will explore performance evaluation under real communication delays of C-V2X devices.

References

- [1] Holger Caesar, Varun Bankiti, Lang Alex H., Vora Sourabh, Liong Venice Erin, Xu Qiang, Krishnan Anush, Yu Pan, Giancarlo Baldan, and Beijbom Oscar. nuscenes: A multi-modal dataset for autonomous driving. In *Proceedings of the IEEE/CVF Conference on Computer Vision and Pattern Recognition*, pages 11618–11628, 2020. 2, 3, 6
- [2] Qi Chen, Xu Ma, Sihai Tang, Jingda Guo, Qing Yang, and Song Fu. F-cooper: Feature based cooperative perception for autonomous vehicle edge computing system using 3d point clouds. In *Proceedings of the 4th ACM/IEEE Symposium on Edge Computing*, pages 88–100, 2019. 3, 7, 8
- [3] Alexey Dosovitskiy, German Ros, Felipe Codevilla, Antonio Lopez, and Vladlen Koltun. Carla: An open urban driving simulator. In *Proceedings of the 1st Annual Conference on Robot Learning*, pages 1–16. PMLR, 2017. 2
- [4] Siqi Fan, Haibao Yu, Wenxian Yang, Jirui Yuan, and Zaiqing Nie. Quest: Query stream for practical cooperative perception. In *2024 IEEE International Conference on Robotics and Automation (ICRA)*, pages 18436–18442, 2024. 3
- [5] Andreas Geiger, Lenz Philip, and Raquel Urtasun. Are we ready for autonomous driving? the kitti vision benchmark suite. In *Proceedings of the IEEE/CVF Conference on Computer Vision and Pattern Recognition*, pages 3354–3361, 2012. 2, 3, 6
- [6] Xiang Hao, Runsheng Xu, and Ma Jiaqi. Hm-vit: Hetero-modal vehicle-to-vehicle cooperative perception with vision transformer. In *2023 IEEE/CVF International Conference ON Computer Vision (ICCV)*, pages 284–295, 2023. 3
- [7] Junjie Huang, Guan Huang, Zheng Zhu, Yun Ye, and Dalong Du. Bevdet: High-performance multi-camera 3d object detection in bird-eye-view. *arXiv preprint arXiv:2112.11790*, 2021. 8
- [8] Daniel Krajzewicz, Jakob Erdmann, Michael Behrisch, and Laura Bieker. Recent development and applications of sumo - simulation of urban mobility. pages 128–138, 2012. 2
- [9] Alex H Lang, Sourabh Vora, Holger Caesar, Lubing Zhou, Jiong Yang, and Oscar Beijbom. Pointpillars: Fast encoders for object detection from point clouds. In *Proceedings of the IEEE/CVF Conference on Computer Vision and Pattern Recognition*, pages 12697–12705, 2019. 6, 7, 8
- [10] Yiming Li, Dekun Ma, Ziyang An, Zixun Wang, Yiqi Zhong, Siheng Chen, and Chen Feng. V2x-sim: Multi-agent collaborative perception dataset and benchmark for autonomous driving. *IEEE Robotics and Automation Letters*, 7(4):10914–10921, 2022. 2, 3
- [11] Yinhao Li, Zheng Ge, Guanyi Yu, Jinrong Yang, Zengran Wang, Yukang Shi, Jianjian Sun, and Zeming Li. Bevdepth: Acquisition of reliable depth for multi-view 3d object detection. In *Proceedings of the AAAI Conference on Artificial Intelligence*, pages 1477–1485, 2023. 6, 7
- [12] Zhiqi Li, Wenhai Wang, Hongyang Li, Enze Xie, Chonghao Sima, Tong Lu, Yu Qiao, and Jifeng Dai. Bevformer: Learning bird’s-eye-view representation from multi-camera images via spatiotemporal transformers. In *European conference on computer vision*, pages 1–18, 2022. 2
- [13] Zechen Liu, Zizhang Wu, and Roland Tóth. Smoke: Single-stage monocular 3d object detection via keypoint estimation. In *Proceedings of the IEEE/CVF Conference on Computer Vision and Pattern Recognition Workshops*, pages 996–997, 2020. 6, 7
- [14] Zhijian Liu, Haotian Tang, Alexander Amini, Xinyu Yang, Huizi Mao, Daniela L Rus, and Song Han. Bevfusion: Multi-task multi-sensor fusion with unified bird’s-eye view representation. In *2023 IEEE international conference on robotics and automation (ICRA)*, pages 2774–2781, 2023. 2
- [15] Yifan Lu, Quanhao Li, Baoan Liu, Mehrdad Dianati, Chen Feng, Siheng Chen, and Yanfeng Wang. Robust collaborative 3d object detection in presence of pose errors. In *2023 IEEE International Conference on Robotics and Automation (ICRA)*, pages 4812–4818, 2023. 8
- [16] Yifan Lu, Yue Hu, Yiqi Zhong, Dequan Wang, Siheng Chen, and Yanfeng Wang. An extensible framework for open heterogeneous collaborative perception. In *The Twelfth International Conference on Learning Representations*, 2024. 3, 7, 8
- [17] Dong-Hee Paek, SEUNG-HYUN KONG, and Kevin Tirta Wijaya. K-radar: 4d radar object detection for autonomous driving in various weather conditions. In *Advances in Neural Information Processing Systems*, pages 3819–3829. Curran Associates, Inc., 2022. 2, 3
- [18] Hualian Sheng, Sijia Cai, Na Zhao, Bing Deng, Jianqiang Huang, Xian-Sheng Hua, Min-Jian Zhao, and Gim Hee Lee. Rethinking iou-based optimization for single-stage 3d object detection. In *European Conference on Computer Vision*, pages 544–561. Springer, 2022. 6, 7
- [19] Shaoshuai Shi, Chaoxu Guo, Li Jiang, Zhe Wang, Jianping Shi, Xiaogang Wang, and Hongsheng Li. Pv-rcnn: Point-voxel feature set abstraction for 3d object detection. In *Proceedings of the IEEE/CVF Conference on Computer Vision and Pattern Recognition*, pages 10529–10538, 2020. 6, 7
- [20] Ziyang Song, Lin Liu, Feiyang Jia, Yadan Luo, Caiyan Jia, Guoxin Zhang, Lei Yang, and Li Wang. Robustness-aware 3d object detection in autonomous driving: A review and outlook. *IEEE Transactions on Intelligent Transportation Systems*, 2024. 2
- [21] Zhiying Song, Tenghui Xie, Hailiang Zhang, Jiabin Liu, Fuxi Wen, and Jun Li. A spatial calibration method for robust cooperative perception. *IEEE Robotics and Automation Letters*, 2024. 4, 5
- [22] Ziyang Song, Lei Yang, Shaoqing Xu, Lin Liu, Dongyang Xu, Caiyan Jia, Feiyang Jia, and Li Wang. Graphbev: Towards robust bev feature alignment for multi-modal 3d object detection. In *European Conference on Computer Vision*, pages 347–366. Springer, 2025. 2

- [23] Pei Sun, Henrik Kretzschmar, Xerxes Dotiwalla, Aurélien Chouard, and Vijaysai Patnaik. Scalability in perception for autonomous driving: Waymo open dataset. In *Proceedings of the IEEE/CVF Conference on Computer Vision and Pattern Recognition*, pages 2443–2451, 2020. 2, 3
- [24] Li Wang, Xinyu Zhang, Wenyuan Qin, Xiaoyu Li, Jinghan Gao, Lei Yang, Zhiwei Li, Jun Li, Lei Zhu, Hong Wang, et al. Camo-mot: Combined appearance-motion optimization for 3d multi-object tracking with camera-lidar fusion. *IEEE Transactions on Intelligent Transportation Systems*, 24(11):11981–11996, 2023. 2
- [25] Li Wang, Xinyu Zhang, Ziyang Song, Jiangfeng Bi, Guoxin Zhang, Haiyue Wei, Liyao Tang, Lei Yang, Jun Li, Caiyan Jia, et al. Multi-modal 3d object detection in autonomous driving: A survey and taxonomy. *IEEE Transactions on Intelligent Vehicles*, 8(7):3781–3798, 2023.
- [26] Lening Wang, Wenzhao Zheng, Yilong Ren, Han Jiang, Zhiyong Cui, Haiyang Yu, and Jiwen Lu. Occsora: 4d occupancy generation models as world simulators for autonomous driving. *arXiv preprint arXiv:2405.20337*, 2024. 2
- [27] Tsun Hsuan Wang, Manivasagam Sivabalan, Ming Liang, Yang Bin, Wenyuan Zeng, and Raquel Urtasun. V2vnet: Vehicle-to-vehicle communication for joint perception and prediction. *European Conference on Computer Vision*, pages 605–621, 2020. 3
- [28] Hao Xiang, Zhaoliang Zheng, Xin Xia, Runsheng Xu, Letian Gao, Zewei Zhou, Xu Han, Xinkai Ji, Mingxi Li, Zonglin Meng, et al. V2x-real: a largs-scale dataset for vehicle-to-everything cooperative perception. *arXiv preprint arXiv:2403.16034*, 2024. 2, 3
- [29] Baowei Xu, Xinyu Zhang, Li Wang, Xiaomei Hu, Zhiwei Li, Shuyue Pan, Jun Li, and Yongqiang Deng. Rpf-net: A 4d radar pillar feature attention network for 3d object detection. In *IEEE International Intelligent Transportation Systems Conference (ITSC)*, pages 3061–3066, 2021. 6, 7
- [30] Runsheng Xu, Yi Guo, Xu Han, Xia Xin, Xiang Hao, and Ma Jiaqi. Openca: an open cooperative driving automation framework integrated with co-simulation. In *IEEE International Intelligent Transportation Systems Conference (ITSC)*, pages 1155–1162, 2021. 2
- [31] Runsheng Xu, Zhengzhong Tu, Xiang Hao, Wei Shao, Bolei Zhou, and Ma Jiaqi. Cobevt: Cooperative bird’s eye view semantic segmentation with sparse transformers. In *CONFERENCE ON ROBOT LEARNING*, pages 989–1000, 2022. 3, 7
- [32] Runsheng Xu, Hao Xiang, Zhengzhong Tu, Xin Xia, Ming-Hsuan Yang, and Jiaqi Ma. V2x-vit: Vehicle-to-everything cooperative perception with vision transformer. In *European Conference on Computer Vision*, pages 107–124. Springer, 2022. 2, 3, 7, 8
- [33] Runsheng Xu, Hao Xiang, Xin Xia, Xu Han, Jinlong Li, and Jiaqi Ma. Opv2v: An open benchmark dataset and fusion pipeline for perception with vehicle-to-vehicle communication. In *2022 International Conference on Robotics and Automation (ICRA)*, pages 2583–2589, 2022. 2, 3
- [34] Runsheng Xu, Xiang Hao, Xu Han, Xia Xin, Zonglin Meng, Chia Ju Chen, Camila Correa Jullian, and Ma Jiaqi. The openca open-source ecosystem for cooperative driving automation research. *IEEE TRANSACTIONS ON INTELLIGENT VEHICLES*, 8(4):2698–2711, 2023. 2
- [35] Runsheng Xu, Xin Xia, Jinlong Li, Hanzhao Li, Shuo Zhang, Zhengzhong Tu, Zonglin Meng, Hao Xiang, Xiaoyu Dong, Rui Song, et al. V2v4real: A real-world large-scale dataset for vehicle-to-vehicle cooperative perception. In *Proceedings of the IEEE/CVF Conference on Computer Vision and Pattern Recognition*, pages 13712–13722, 2023. 2, 3, 7
- [36] Yan Yan, Yuxing Mao, and Bo Li. Second: Sparsely embedded convolutional detection. *Sensors*, 18(10):3337, 2018. 6, 7
- [37] Lei Yang, Tao Tang, Jun Li, Peng Chen, Kun Yuan, Li Wang, Yi Huang, Xinyu Zhang, and Kaicheng Yu. Bevheight++: Toward robust visual centric 3d object detection. *arXiv preprint arXiv:2309.16179*, 2023. 6, 7
- [38] Lei Yang, Kaicheng Yu, Tao Tang, Jun Li, Kun Yuan, Li Wang, Xinyu Zhang, and Peng Chen. Bevheight: A robust framework for vision-based roadside 3d object detection. In *Proceedings of the IEEE/CVF Conference on Computer Vision and Pattern Recognition*, pages 21611–21620, 2023. 6, 7
- [39] Lei Yang, Xinyu Zhang, Jun Li, Li Wang, Minghan Zhu, Chuang Zhang, and Huaping Liu. Mix-teaching: A simple, unified and effective semi-supervised learning framework for monocular 3d object detection. *IEEE Transactions on Circuits and Systems for Video Technology*, 33(11):6832–6844, 2023. 2
- [40] Xiaoqing Ye, Mao Shu, Hanyu Li, Yifeng Shi, Yingying Li, Guangjie Wang, Xiao Tan, and Errui Ding. Rope3d: The roadside perception dataset for autonomous driving and monocular 3d object detection task. In *Proceedings of the IEEE/CVF Conference on Computer Vision and Pattern Recognition*, pages 21341–21350, 2022. 6
- [41] Tianwei Yin, Xingyi Zhou, and Philipp Krahenbuhl. Center-based 3d object detection and tracking. In *Proceedings of the IEEE/CVF Conference on Computer Vision and Pattern Recognition*, pages 11784–11793, 2021. 6, 7
- [42] Haibao Yu, Yizhen Luo, Mao Shu, Yiyi Huo, Zebang Yang, Yifeng Shi, Zhenglong Guo, Hanyu Li, Xing Hu, Jirui Yuan, et al. Dair-v2x: A large-scale dataset for vehicle-infrastructure cooperative 3d object detection. In *Proceedings of the IEEE/CVF Conference on Computer Vision and Pattern Recognition*, pages 21361–21370, 2022. 2, 3, 7
- [43] Haibao Yu, Wenxian Yang, Hongzhi Ruan, Zhenwei Yang, Yingjuan Tang, Xu Gao, Xin Hao, Yifeng Shi, Yifeng Pan, Ning Sun, et al. V2x-seq: A large-scale sequential dataset for vehicle-infrastructure cooperative perception and forecasting. In *Proceedings of the IEEE/CVF Conference on Computer Vision and Pattern Recognition*, pages 5486–5495, 2023. 2, 3
- [44] Haibao Yu, Yingjuan Tang, Enze Xie, Jilei Mao, Ping Luo, and Zaiqing Nie. Flow-based feature fusion for vehicle-infrastructure cooperative 3d object detection. *Advances in Neural Information Processing Systems*, 36, 2024. 3
- [45] Haibao Yu, Wenxian Yang, Jiaru Zhong, Zhenwei Yang, Siqi Fan, Ping Luo, and Zaiqing Nie. End-to-end au-

- tonomous driving through v2x cooperation. *arXiv preprint arXiv:2404.00717*, 2024. 3
- [46] Xinyu Zhang, Li Wang, Jian Chen, Cheng Fang, Lei Yang, Ziyang Song, Guangqi Yang, Yichen Wang, Xiaofei Zhang, Qingshan Yang, and Jun Li. Dual radar: A multi-modal dataset with dual 4d radar for autonomous driving. *arXiv preprint arXiv:2310.07602*, 2023. 2, 3
- [47] Tong Zhao, Yichen Xie, Mingyu Ding, Lei Yang, Masayoshi Tomizuka, and Yintao Wei. A road surface reconstruction dataset for autonomous driving. *Scientific data*, 11(1):459, 2024. 2
- [48] Tong Zhao, Lei Yang, Yichen Xie, Mingyu Ding, Masayoshi Tomizuka, and Yintao Wei. Roadbev: Road surface reconstruction in bird’s eye view. *IEEE Transactions on Intelligent Transportation Systems*, 25(11):19088–19099, 2024. 2
- [49] Jiaru Zhong, Haibao Yu, Tianyi Zhu, Jiahui Xu, Wenxian Yang, Zaiqing Nie, and Chao Sun. Leveraging temporal contexts to enhance vehicle-infrastructure cooperative perception. *arXiv preprint arXiv:2408.10531*, 2024. 3
- [50] Walter Zimmer, Gerhard Arya Wardana, Suren Sritharan, Xingcheng Zhou, Rui Song, and Alois C Knoll. Tumoratraf v2x cooperative perception dataset. In *Proceedings of the IEEE/CVF Conference on Computer Vision and Pattern Recognition*, pages 22668–22677, 2024. 3